Journal of Materials Science: Materials in Electronics (2019) 30:17032–17039
https://doi.org/10.1007/s10854-019-02045-x

The investigation of effects of (Fe_2O_4-PVP) organic-layer, surface states, and series resistance on the electrical characteristics and the sources of them

Seçkin Altındal Yerişkin[1]

Received: 21 May 2019 / Accepted: 13 August 2019 / Published online: 13 September 2019
© Springer Science+Business Media, LLC, part of Springer Nature 2019

Abstract

In this work, Au/n-Si (MS) structures with and without (Fe_2O_4-doped PVP) interlayer were prepared with the same conditions to see effects of organic layer on the electrical characteristics and conduction mechanisms. For this aim, I–V and Z–V measurements of them were carried out at room temperature. The saturation current (I_s), ideality factor (n), barrier height (Φ_B(I–V)), series (R_s) and shunt (R_{sh}) resistances, and rectifying rate ($RR = I_F/I_R$) of them were extracted from the I–V data as 2.90×10^{-8} A, 1.699, 0.741 eV, 1.58 kΩ, 25.7 MΩ, 1.45×10^4 for MS and 2.30×10^{-9} A, 1.634, 0.806 eV, 1.17 kΩ, 103 MΩ, 9.01×10^4 for MPS, respectively. The values of interface states (N_{ss}) were also extracted from the I–V data at forward bias by considering voltage dependent BH and n, and it is found that they increase from the mid-gap of semiconductor towards the conductance band. The values of doping atoms (N_D), Fermi-energy (E_F), and (Φ_B(C–V)) were also acquired from the C^{-2}–V plots at reverse bias as 9.08×10^{14} cm^{-3}, 0.258 eV, 0.914 eV for MS and 7.650×10^{14} cm^{-3}, 0.263 eV, 0.981 eV, for MPS structure, respectively. It is clear that the (Fe_2O_4-PVP) interlayer leads to decreases in R_s, N_{ss}, leakage current and increase in rectifying rate (RR), R_{sh} and BH, so that it can used in place of the conventional oxide or insulator layer.

1 Introduction

MIS and MPS type electronic devices consist of an interfacial oxide and polymer layer between metal and semiconductor, and many defects or impurities may be occurred during the elaboration/fabrication of them. They are usually called as surface/interface states/traps (N_{ss}/D_{it}) and may alter the performance of these devices. These states are usually originated from dangling bounds at surface of semiconductor and chemical composition of the interface [1–5]. The charges in these traps and dislocations may be stored or released under electric field [6–9]. Therefore, the value of admittance ($Y = 1/Z = G + j\omega C$) increases by decreasing frequency and these changes in them become more pronounced at lower frequencies depending on the life-times (τ) of the N_{ss} and alternating ac signal. In other words, there are many types of the N_{ss} with various lifetimes, especially at low-moderate frequencies [5–10].

The existence of a native/deposited interlayer such as insulator, ferroelectric and polymer at junction, MS structure is converted into the MIS, MFS and MPS structures. The thickness, its homogeneity and dielectric constant of interlayer are also more effective on the performance of these devices as much as barrier inhomogeneity [6–8]. Therefore, the n value acquired from the slope of forward bias Ln(I)–V curve becomes much higher than unity because of the existence of native or deposited interlayer, N_{ss}, inhomogeneous of BH, and tunneling of charge carriers through BH [6–9, 11–15]. Therefore, main electrical of these structures obtained from the forward I–V based on TE theory and reverse bias C–V data may be considerably different depending on voltage, interlayer, and the nature of measured method. Therefore, in application, the obtained experimental results may be considerably different from the ideal case. Additionally, on the base of TE theory, the value of BH does not include the electric field and so the value of BH becomes a function of applied bias voltage [6–8, 16–19]. The magnitude of n is also an indicator of compliance to TE theory and its higher values imply a deviation from the TE theory ($n \approx 1$) and it depend on various factors such as V, depletion layer width ($W_d = \sim \sqrt{1/N}$), the permittivity of interlayer (ε_i), and its thickness (d_i) [6–8]. The existence

✉ Seçkin Altındal Yerişkin
seckin.ay19@gmail.com

[1] Department of Chemical Engineering, Faculty of Engineering, Gazi University, Ankara, Turkey

of many low-barriers at M/S interface, some low-energetic electrons can be tunneled via these barriers and cause an increment in n values.

Both the R_s and R_{sh} of electronic devices are also more effective on the conduction mechanism and then on the performance of them. In general, R_s may be rooted from the ohmic and Schottky contacts of the device, the used probe wires to get contacts, the resistance of the bulk semiconductor, and inhomogeneity doping atoms [7, 9]. But, the value of R_{sh} may be rooted from the physical defects, grain boundaries, and leakage current, and probe wires to the ground. R_s value can be determined by many methods from the I–V data. Among these methods, the commonly used ones which provide an opportunity for comparison are Ohm's law [7], Norde [20] and Cheung functions [21], and modified Norde functions by Bohlin [22]. But, Ohm-law and Cheung functions are the easiest, exact and reliable ones from the high forward biases region because it realizes in this region and deviates from linearity of LnI–V plot and the bending of the C–V plot at accumulation region. According to Ohm's law, the voltage dependence resistance of the structure ($R_i = dV_m/dI_m$) and Nicollian-Brews method ($R_i = G_m/(G_m^2 + (\omega C_m)^2)$, can easy to calculate by utilizing the forward measured I–V and impedance (C–V and G/ω–V) data, respectively. But, the real value of R_s corresponds to high-forward biases and strong accumulation region of C/G–V plot, respectively.

The main aim of this study is to compare the basic electronic parameters of fabricated the Au/n-Si (MS) and Au/(Fe_2O_4-doped PVP)/n-Si (MPS) structures by considering the effects of (Fe_2O_4-doped PVP) organic layer, N_{ss}, R_s, and their possible sources. For this aim, both the I–V and C/G–V (at 1 MHz) measurements were performed. In addition, the main electronic parameters of these two structures such as n, BH and R_s were obtained using the different methods, namely TE theory, Cheung's and Nicollian-Brews methods and compared with each other. All these results confirm that the (Fe_2O_4-doped PVP) interfacial organic/polymer layer lead to a considerably decreases in R_s, N_{ss}, leakage current and an increase in rectifying rate (RR), R_{sh} and BH when compared with reference device (MS).

2 Experimental details

In order to specify the effects of (Fe_2O_4-doped PVP) organic interlayer on the performance of the conventional MS structure, the Au/n-Si (MS) structures with and without this organic interlayer were performed on the P-doped (n-Si) wafer having (100) float zone, 350 µm thickness, 2" diameter, and ~ 1.078×10^{15} cm^{-3} dopant donor concentration atoms in same conditions. For the fabrication of the MS and MPS structures, two quarter n-Si wafers were dipped in ammonium-peroxide at 50 s to remove native-oxide layer and organic impurities on the two side of wafers and then wafers etched in the (H_2SO_4:H_2O_2:H_2O = 3:1:1) solutions and (HCl:H_2O = 1:1) for 1 min, respectively. After that, wafers rinsed in ultra-pure water and then N_2 gas used for drying. After the cleaning processes, two quarter n-Si wafers were rinsed in deionized water and then dried in N_2 gas. After that these two n-Si wafers were transferred into high-vacuum metal evaporation system and then 150 nm thickness of high-pure Au (99.999%) was evaporated onto the whole back side of the n-Si wafers at ~ 10^{-6} Torr. In order to get low-resistivity or good ohmic contact these two wafers were annealed at 550 °C for 5 min in a N_2 atmosphere. Additionally, the current–voltage plots of them were measured by using Keithley-2400 source-meter and they show a good linear behaviour which is an evidence to perform a good ohmic contact. Then, high-pure Au circular dots with 1 mm diameter and 150 nm thickness were deposited on the front of first quarter n-Si wafer. In this way, the fabrication of Au/n-Si (MS) structures was completed. After that, utilizing electrospinning method, the growth of the prepared (Fe_2O_4-doped PVP) organic solution was realized on the front of second quarter n-Si wafer. The organic layer thickness was predicted as 22 nm from the interlayer capacitance (C_i). Immediately, high-pure Au (99.999%) circular dots with 1 mm diameter and 150 nm thickness were deposited on the (Fe_2O_4-doped PVP) organic layer at 10^{-6} Torr evaporation system. The schematic diagrams of them were also given in Fig. 1. The I–V and C/G–V measurements were realized by Keithley-2400 source-meter and HP4192A impedance analyser (5 Hz–13 MHz), respectively. All measurements were done by used a microcomputer through an IEEE-488 ac/dc converter card.

3 Results and discussions

3.1 Forward and reverse bias I–V characteristics

Figure 2 shows the semi-logarithmic I–V curves of the Au/n-Si (MS) and Au/(Fe_2O_4-doped PVP)/n-Si (MPS) structures between ± 3 V interval by 20 mV steps. As seen in the Fig. 2, the lnI–V curve for two structures exhibits typical diode behavior with a good rectifying rate. In addition, lnI–V plots have liner part in the intermediate forward bias voltage up to ~ 0.5 V and then deviate from linearity because of the organic interlayer (Fe_2O_4-doped PVP) and Rs effects. Because, the applied biases across the structure will be shared by R_s, organic and depletion layers, but R_s effect at low and moderate bias voltages can be neglected low.

Since electronic devices have both R_s and n is greater than unity, TE theory can also be used to determine electrical parameters, and in this case the I–V relation (≥ 3 kT/q) is expressed as below [6–8].

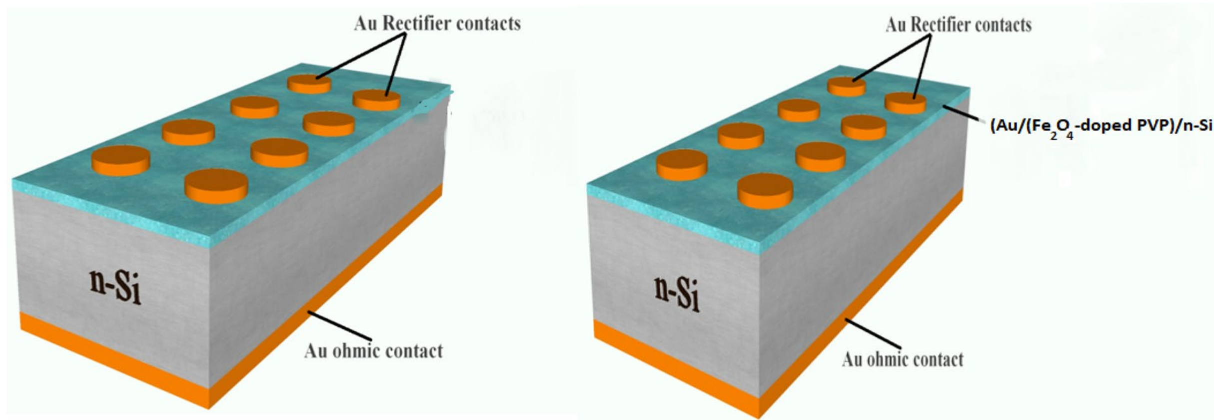

Fig. 1 Schematic diagram of the Au/n-Si (MS) and Au/(Fe_2O_4-doped PVP)/n-Si (MPS) structures, respectively

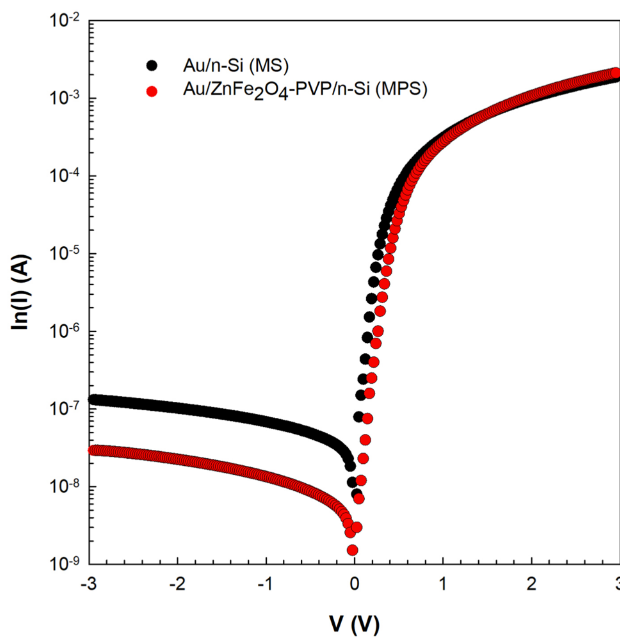

Fig. 2 The semi-logarithmic I–V plots of the MS and MPS structures

$$I = AA^{*}T^{2}\exp(-\frac{q}{kT}\Phi_{Bo})\left[\exp\left(\frac{q(V-IR_{s})}{nkT}\right)-1\right] = \mathrm{I}_{O}\left[\exp\left(\frac{qV_{D}}{nkT}\right)-1\right] \quad (1)$$

In Eq. 1, A^* is the effective Richardson constant (112 A/cm^2 K^2 for n-Si), the products of IR_s is the voltage drop across the R_s and the other quantities are most-known in the evaluable literature. Both I_o and n values can be extracted from the intercepts and slopes of lnI–V plot [$Ln(I) = Ln(I_o) + (q/nkT)V$] as following through the relation by using Eq. 1, respectively [6–8]:

$$n = \frac{q}{kT}\left(\frac{dV}{d(\ln I)}\right) = \left(\mathrm{d_i}/\varepsilon_{\mathrm{i}}\right)\left(\varepsilon_{\mathrm{s}}/\mathrm{W_d} + \mathrm{qN_{ss}}\right) \quad (2)$$

Thus, Φ_{Bo} was extracted from Eq. 1 by using the acquired I_o value and the diode area (A) for MS and MPS structures through the equation below [6–8].

$$\Phi_{Bo} = \frac{kT}{q}Ln\left(\frac{AA^{*}T^{2}}{I_{0}}\right) \quad (3)$$

I_o, n, Φ_{Bo}, and RR values were extracted from the Ln(I)–V plots as 2.9×10^{-8}A, 1.699, 0.741 eV, and 1.45×10^4 for the MS and 2.30×10^{-9} A, 1.634, 0.806 eV, and 9.01×10^4 for MPS structure and they are tabulated in Table 1, respectively. It is clear that these values of n are higher than unity due to the lower BHs/patches at around mean BH, a spatial distribution of N_{ss} at (Fe_2O_4-PVP)/n-Si interface, and organic layer. Many charge carriers (electron and holes) with low energies can easily pass across these patches and increase the n values. According to Saad and Kassis [23], the other reason of high value of n in these structures is the result of conduction dominated by interface recombination.

Table 1 A comparison of some basic electrical parameters of the MS and MPS structures extracted from the Ln(I)-V and Cheung's functions at room temperature

	Ln(I)-V				Cheung dV/dLn(I)-I		Cheung H(I)-I	
Sample	I_o (A)	n	Φ_{Bo} (eV)	RR	n	Rs (kΩ)	Rs (kΩ)	Φ_b (eV)
MS	2.9×10^{-8}	1.699	0.741	1.45×10^4	5.40	1.372	1.32	0.606
MPS	2.30×10^{-9}	1.634	0.806	9.01×10^4	4.40	1.266	1.21	0.652

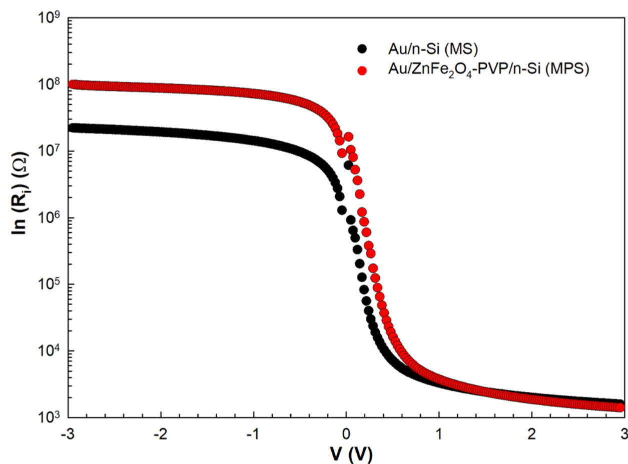

Fig. 3 The R_i–V plots of the Au/n-Si (MS) and Au/(Fe_2O_4-doped PVP)/n-Si (MPS) structures

The n value is a measure of TE theory and higher values of it deviates the structure from TE. The voltage dependent resistance ($R_i = V_i/I_i$) of these structures can be extracted from the Ohm's law, but the real R_s value and R_{sh} of them corresponds to adequately high forward and reverse bias voltage. Therefore, the values of R_s and R_{sh} were calculated as 1.58 kΩ and 25.7 MΩ for MS and 1.17 kΩ and 103 MΩ for MPS at ± 3 V (Fig. 3), respectively.

The main diode parameters (I_o, n, Φ_{Bo}) can also be determined by using Cheung functions from the concave curvature forward bias region as following equations [21]:

$$\frac{dV}{d(InI)} = IR_s + \left(\frac{nkT}{q}\right) \tag{4a}$$

$$H(I) = V - \frac{nkT}{a} In\left(\frac{I}{AA^*T^2}\right) = IR_s + n\phi_B \tag{4b}$$

Both the dV/dIn(I) and H(I) versus I plots of two structures were drawn by using Eq. 4a and 4b, and were represented in Fig. 4a and b, respectively. As presented in Fig. 4a and b, related plots have a distinct linear behavior. Thus, as shown in Eq. 4a, the slopes and intercept points of the dV/dIn(I) versus I plots are exactly equal to the real R_s values and nkT/q. Thus, the value of R_s and n were found as 1.372 kΩ and 5.40 for MS and 1.266 kΩ and 4.40 for MPS structures, respectively. By using these values of n, H(I) versus I plots (Fig. 4b) were also drawn using Eq. 4b. The slopes and intercepts of these plots are corresponding to R_s and $n\Phi_B$, respectively. Thus, both the values of R_s and BH were calculated as 1.32 kΩ and 0.606 eV for MS and 1.21 kΩ and 0.652 eV for MPS structure respectively. These values of n, R_s and Φ_b obtained by Cheung functions are in reasonably close agreement with each other. But, observed

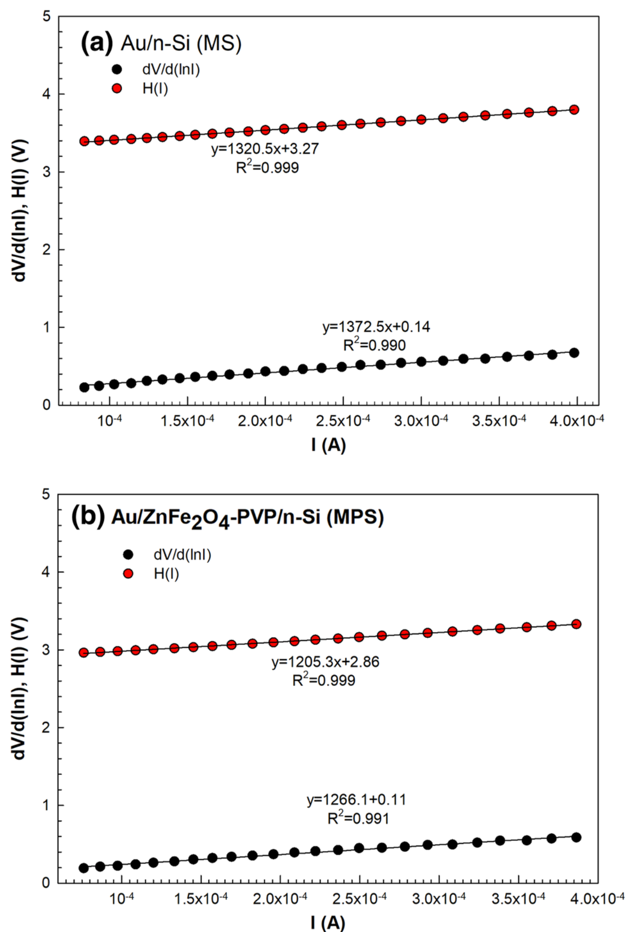

Fig. 4 dV/d(ln I) and H(I) versus I plots of the MS and MPS structures

some discrepancy between these parameters obtained from TE theory and Cheung's functions is the result of the voltage dependent of them and the nature of measurements methods.

Figure 5 shows the double logarithmic I_F–V_F plots of two structures, which are related to the characteristic of the conduction process of dominant charge over the barrier. As shown in Fig. 5, the In(I_F)–In(V) plot has three linear regions with different slopes and they called as I, II, and III which are correspond to low, intermediate and high forward bias voltages, respectively. It is clear that in these regions, Ln(I_F)–ln(V_F) plots have a power-law behavior ($I \sim V^{m+1}$) with different slope values (m) which is directly equal to the slope of these linear regions. Thus, the value of m for regions I, II, and III were found as 1.976, 3.915, and 1.846 for MS and 1.701, 5.002, and 2.144 for MPS structure respectively. Both in I and III regions for two structures, current-conduction is the space-charge-limited-current (SCLC) mechanism because m is closer 2, due to an increase in electrons injected from the electrode to the interlayer, and so leads to filling up of traps and a rise in

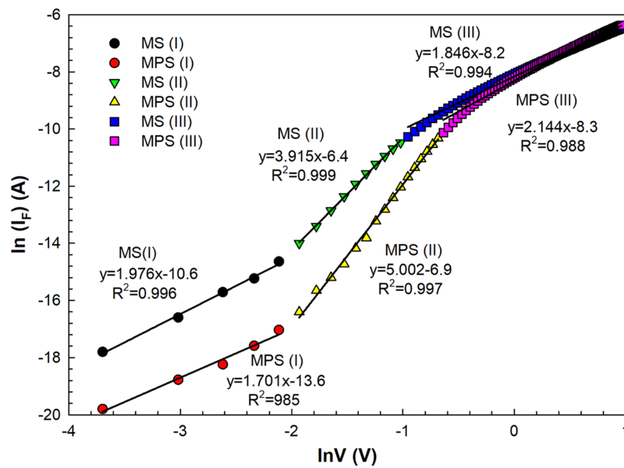

Fig. 5 $Ln(I_F–V_F)$ plots of the Au/n-Si (MS) and Au/(Fe_2O_4-doped PVP)/n-Si (MPS) structures

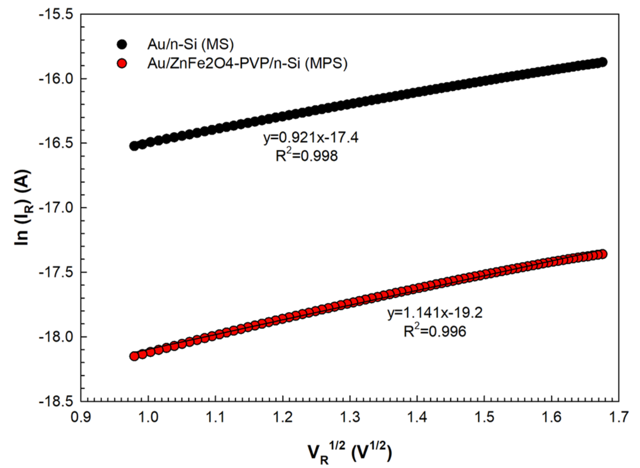

Fig. 6 $Ln(I_r)–V_R^{0.5}$ plots of the Au/n-Si (MS) and Au/(Fe_2O_4-doped PVP)/n-Si (MPS) structures

space charges [24–26]. But, for region II m is larger than 2 for MS and MPS structure and so it has been interpreted as an indicator of trapped-charge-limited current (TCLC) with an exponential interface states/traps distribution.

As shown in Fig. 2, the reverse bias $I_R–V_R$ plots for these two structures have not a soft or non-saturation behavior and the values of I_R increases with increasing V_F or electric field. Such behavior of reverse bias current suggests that either Poole–Frenkel emission (PFE) or Schottky emission (SE) is dominant mechanisms in the MS and MPS structures. Therefore, $\ln(I_R)–V_R^{0.5}$ plots of them were drawn and given in Fig. 6 to determine possible current-transport mechanisms (CTMs/CCMs) in the MS and MPS structures.

According to the PFE and SE mechanisms, the relation between I_R and V_R is expressed as follows, respectively [7, 24]:

$$I_R = I_o \exp\left(\frac{\beta_{PF} V^{0.5}}{kTd^{0.5}}\right) \tag{5a}$$

$$I_R = I_o \exp\left(\frac{\beta_{SC} V^{0.5}}{kTd^{0.5}}\right) \tag{5b}$$

In Eq. 5a and 5b, d is the interfacial layer thickness, β_{PF} and β_{SC} are PFE and SE coefficients and theoretical value of them is given as follows [7]:

$$2\beta_{SC} = \beta_{PF} = \left(\frac{q^2}{\pi\varepsilon_0\varepsilon_i}\right)^{0.5} \tag{5c}$$

Here ε_i and ε_o (8.85×10^{-12} F/m) are the dielectric of interlayer and vacuum, respectively. The theoretical β_{PF} and β_{SC} values are calculated as 3.89×10^{-5} $eV^{-1}m^{0.5}V^{0.5}$ and 3.73×10^{-5} $m^{0.5}V^{0.5}$, respectively. As seen in Fig. 6, the $\ln(I_R)–V_R^{0.5}$ plot shows good linear behavior for these two structures. The experimental value of β was obtained from the slope of these plots as 1.46×10^{-5} $eV^{-1}m^{0.5}V^{0.5}$ for MS and 3.12×10^{-5} $m^{0.5}V^{0.5}$ for MPS structures, respectively. These theoretical and experimental values of β show that the CCM is dominated by SE in the MS structure, whereas PFE is dominated in MPS structure due to the current conduction is composed of the metal into conductive dislocations via surface states or traps [7].

In order to determine whether or not the passivated (Fe_2O_4-PVP) interfacial organic layer effect N_{ss}, the energy-dependent of the N_{ss} was obtained from the $I_F–V_F$ plots by using following Eq. 6a, 6b for MS and MPS structure by considering V dependent BH and n were given in Fig. 7. The energy-dependent profile of the N_{ss} can be obtained from Eq. 2 as follows [7, 8].

$$N_{ss}(V) = \frac{1}{q}\left[\frac{\varepsilon_i}{d_i}(n(V)-1) - \frac{\varepsilon_s}{W_D}\right] \tag{6a}$$

Here, the depletion layer width acquired from the C^{-2}–V plots at reverse biases is denoted by W_D. The values of N_{ss} with respect to the bottom of conductance band (E_c) are expressed as follows.

$$E_c - E_{ss} = q\left(\Phi_e - V\right) \tag{6b}$$

Here, Φe $[(1–n^{-1})V]$ is the effective BH. In Fig. 7, the increment of N_{ss} values from the mid-gap of Si towards bottom edge of E_c were almost seen as exponentially. MPS structure's N_{ss} values are also substantially low when compared with MS structure in the whole energy range.

These results are validated that the (Fe_2O_4-doped PVP) organic interlayer enhanced the performance of MS because of incorporation in PVP lattices reduces many oxygen vacancies and leads to lower density of charge carriers, which

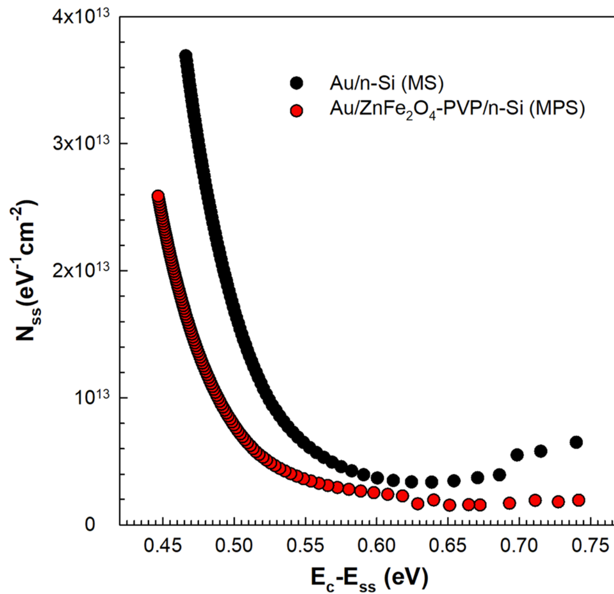

Fig. 7 N_{ss}–(E_c–E_{ss}) of the MS and MPS structures

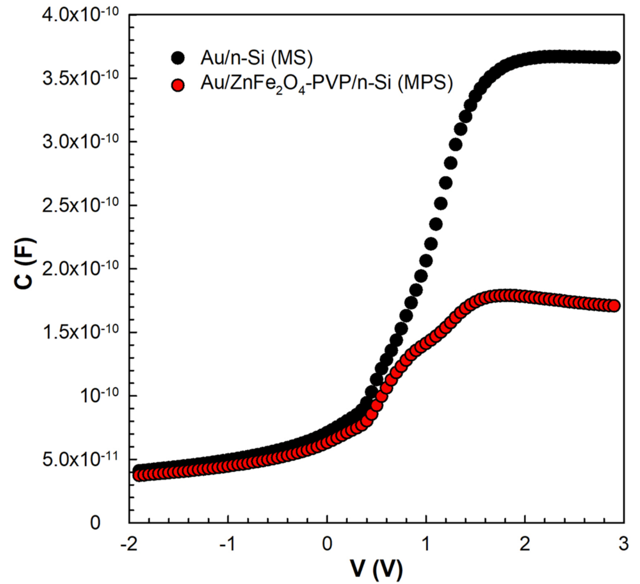

Fig. 8 C–V plots of the MS and MPS structures

can also effectively increase the BH [3, 16, 27–34]. These mean values of N_{ss} (~ 10^{13} eV^{-1} cm^{-2}) are suitable for these structures.

3.2 Forward and reverse bias C–V and G/ω–V Characteristics

The other electrical parameters such as the density of donor atoms (N_D), Fermi energy (E_F), Φ_B(C–V), W_D, maximum electric field (E_m), R_s, and N_{ss} were obtained from the C–V and G/ω–V characteristics (Figs. 8 and 9) for 1 MHz. As shown in these curves, these plots have three regimes which are accumulations, depletions, and inversions like MIS structure.

The C^{-2}–V plots of the MS structures with Fe_2O_4-doped PVPAu/n-Si interlayer and without interlayer were given in Fig. 10. These plots have a well linear zone in wide biases interval for two structures.

The values of N_D, E_F, Φ_B(C–V), W_D, and E_m were calculated from the slopes and intercepts at Fig. 10 as 9.08 × 10^{14} cm^{-3}, 0.258 eV, 0.914 eV, 9.53 × 10^{-5} cm, and 1.32 × 10^4 V/cm for MS and 7.65 × 10^{14} cm^{-3}, 0.263 eV, 0.981 eV, 1.29 × 10^{-4} cm, and 1.27 × 10^4 V/cm for MPS structure by using following equations [6, 7]:

$$\left[N_D = 2/q_{so}A^2\left(\frac{dC^{-2}}{dV}\right)\right] \tag{7a}$$

$$E_F = \frac{kT}{q}\ln\left(\frac{N_C}{N_D}\right) \tag{7b}$$

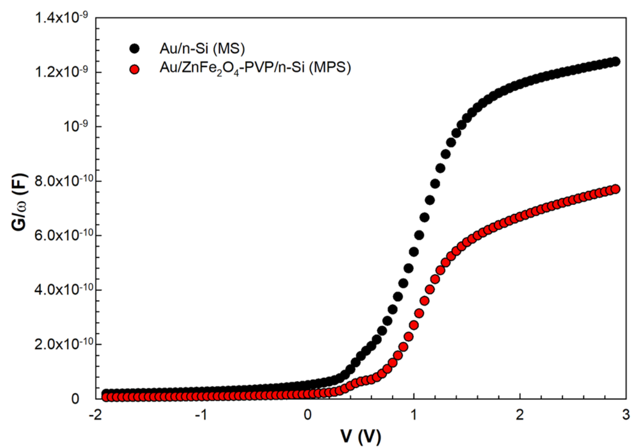

Fig. 9 G/ω–V plots of the MS and MPS structures

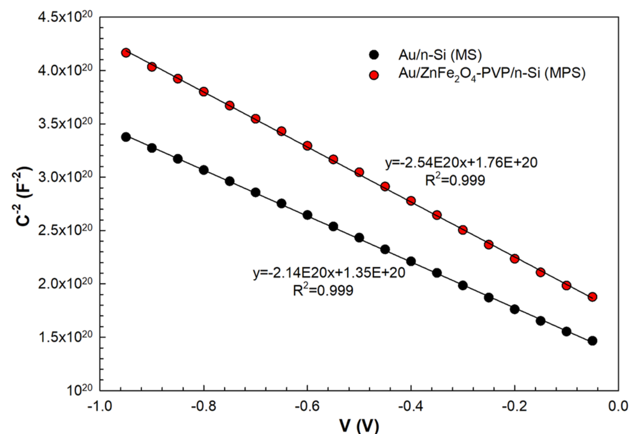

Fig. 10 C^{-2}–V plots of the MS and MPS structures

$$E_m = \left[\left(2qN_DV_o\right)/\left(\varepsilon_s\varepsilon_o\right)\right]^{1/2} \quad (8a)$$

$$W_D = \left(2\varepsilon_s V_D / qN_D\right)^{1/2} \quad (8b)$$

Hence, the Φ_B(C–V) value can be derived from the following equation [7].

$$_B(C - V) = V_o + \frac{kT}{q} + E_F \quad (9)$$

In Eqs. 7 and 8; the quantities of ε_s, N_C ($=2.8 \times 10^{19}$ cm^{-3}), V_D are the dielectric permittivity of Si (11.8), the density of states in the E_c, and diffusion potential ($=V_o + kT/q$) [7], respectively. The obtained BH from the I_F–V_F characteristics is lower than at about E_F energy obtained from the C_R–V_R data for 1 MHz for two type structures due to the result of voltage, measurement method and barrier in-homogeneities, because the apparent BH from the M to S is lower than the S to M for charge carriers. Additionally, under forward bias, current follows the line through lower BHs since the barrier is inhomogeneous and so leads to increase in current or decrease in Φ_{Bo}. So, that BH is certainly the nominal arithmetic mean of these patches [27].

The value of R_s arise from many reasons such as the back and front contacts formation, bulk resistivity, impurities or dislocations, probe wires and in-homogeneity of doping atoms and interlayer and it is more effective on the C–V and G/ω–V measurements at high frequencies at accumulation region [35–39]. Thus, the voltage dependent Ri of these two structures for 1 MHz were also obtained using equation below presented by Nicollian and Brews and indicated in Fig. 11 [9]:

$$R_s = \frac{G_m}{G_m^2 + \left(\omega C_m\right)^2} \quad (10)$$

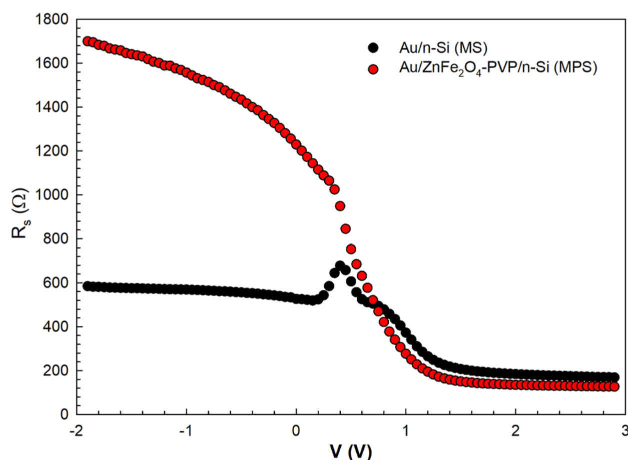

Fig. 11 R_i–V plots of the MS and MPS structures

In Eq. 10; the measured G and C values for biases are G_m and C_m. But, the real value of R_s corresponds to R_i value at strong accumulation region for a MIS or MOS structure. Thus, the real value of R_s was calculated from Eq. 10 as 168 Ω and 126 Ω for MS and MPS structures at 3 V, respectively. Similar results have been reported by various researchers [40–42].

4 Conclusions

In the present study, Au/n-Si structures with and without Fe_2O_4-doped PVP interlayer were investigated at same conditions to determine the effects of (Fe_2O_4-doped PVP) organic interfacial layer on the I–V, C–V and G–V characteristics as well as performance of the MS structure at room temperature. For these purposes, both the I–V and C/G–V (at 1 MHz) measurements were performed at room temperature. In this way, the values of n, BH and R_s were obtained using the different experimental measurement methods and also calculated methods namely TE theory, Cheung's and Nicollian-Brews methods and compared with each other. When these experimental results are compared for MS and MPS structures, it is seen that the used (Fe_2O_4-doped PVP) interlayer at M/S interface leads to a quite decreases in R_s, N_{ss}, leakage current and an increase in rectifying rate (RR), R_{sh} and BH. The obtained BH from the forward bias I–V data was found lower than its obtained values from the C_R–V_R data for 1 MHz for two type structures and it is attributed to the voltage and measurement method, because the apparent BH from the M to S is lower than the semiconductor to metal for charge carriers. In conclusion, the interfacial organic layer (Fe_2O_4-doped PVP) significantly improves the performance of the MS structure and so it can be successfully used instead of traditional insulator layer from the point of easy growth processes with lower cost and energy consumption, low weight per molecule and flexibility.

References

1. G. Ersöz, İ. Yücedağ, Y. Azizian-Kalandaragh, İ. Orak, Ş. Altındal, Investigation of electrical characteristics in Al/CdS-PVA/p-Si (MPS) structures using impedance spectroscopy method. IEEE Trans. Electron Devices **63**, 2948–2955 (2016)
2. M.S. Pratap Reddy, L. Jung-Hee, J. Ja-Soon, Frequency dependent series resistance and interface states in Au/bio-organic/n-GaN Schottky structures based on DNA biopolymer. Synth. Met. **185–186**, 167–171 (2013)
3. S. Altındal Yerişkin, M. Balbaşı, İ. Orak, The effects of (graphene doped-PVA) interlayer on the determinative electrical parameters of the Au/n-Si (MS) structures at room temperature. J. Mater. Sci. **28**, 14040–14048 (2017)
4. P.R. Sekhar Reddy, V. Janardhanam, I. Jyothi, V. Shim-Hoon Yuk, Rajagopal Reddy, Jae-Chan Jeong, Sung-Nam Lee, Chel-Jong Choi, Modification of Schottky barrier properties of Ti/p-type

InP Schottky diode by polyaniline (PANI) organic interlayer. J. Semicond. Technol. Sci. **16**, 664–674 (2016)
5. M. Sharma, S.K. Tripathi, Frequency and voltage dependence of admittance characteristics of Al/Al_2O_3/PVA:n-ZnSe Schottky barrier diodes. Mater. Sci. Semicond. Process. **41**, 155–161 (2016)
6. E.H. Rhoderick, R.H. Williams, *Metal-semiconductor contacts*, 2nd edn. (Clarendon Press, Oxford, 1988)
7. S.M. Sze, K.K. Ng, *Physics of semiconductor devices*, 3rd edn. (Wiley, New Jersey, 2006)
8. H.C. Card, E.H. Rhoderick, Studies of tunnel MOS diodes I. Interface effects in silicon Schottky diodes. J. Phys. D **4**, 1589–1601 (1971)
9. E.H. Nicollian, J.R. Brews, *MOS (metal oxide semiconductor) physics and technology* (Wiley, New York, 1982)
10. Y.P. Song, R.L. Van Meirhaeghe, W.H. Laflere, F. Cardon, On the difference in apparent barrier height as obtained from capacitance-voltage and current-voltage-temperature measurements on Al/p-InP Schottky barriers. Solid States Electron. **29**, 633–638 (1986)
11. W. Mönch, Barrier heights of real Schottky contacts explained by metal-induced gap states and lateral inhomogeneities. J. Vac. Sci. Technol., B **17**, 1867–1876 (1999)
12. J.H. Werner, H.H. Güttler, Barrier inhomogeneities at Schottky contacts. J. Appl. Phys. **69**, 1522–1533 (1991)
13. M.S.P. Reddy, H.S. Kang, J.H. Lee, V.R. Reddy, J.S. Jang, Electrical properties and the role of inhomogeneities at the polyvinylalcohol/n-InP Schottky barrier interface. J. Appl. Polym. Sci. **131**, 39773 (2014)
14. E. Arslan, Ş. Altındal, S. Özçelik, E. Özbay, Tunneling current via dislocations in Schottky diodes on AlInN/AlN/GaN heterostructures. Semicond. Sci. Technol. **24**, 075003 (2009)
15. F.A. Padovani, R. Stratton, Field and thermionic-field emission in Schottky barriers. Solid State Electron. **9**, 695–707 (1966)
16. S. Demirezen, S. Altındal Yerişkin, A detailed comparative study on electrical and photovoltaic characteristics of Al/p–Si photodiodes with coumarin–doped PVA interfacial layer: the effect of doping concentration. Polym. Bull. (2019). https://doi.org/10.1007/s00289-019-02704-3
17. H.H. Güttler, J.H. Werner, Influence of barrier inhomogeneities on noise at Schottky contacts. Appl. Phys. Lett. **56**, 1113–1115 (1990)
18. R.T. Tung, Recent advances in Schottky barrier concepts. Mater. Sci. Eng., R **35**, 1–138 (2001)
19. J.P. Sullivan, R.T. Tung, M.R. Pinto, W.R. Graham, Electron transport of inhomogeneous Schottky barriers: a numerical study. J. Appl. Phys. **70**, 7403–7424 (1991)
20. H. Norde, A modified forward *I–V* plot for Schottky diodes with high series resistance. J. Appl. Phys. **50**, 5052–5053 (1979)
21. S.K. Cheung, N.W. Cheung, Extraction of Schottky diode parameters from forward current-voltage characteristics. Appl. Phys. Lett. **49**, 85–87 (1986)
22. K.E. Bohlin, Generalized Norde plot including determination of the ideality factor. J. Appl. Phys. **60**, 1223–1224 (1986)
23. M. Saad, A. Kassis, Analysis of illumination-intensity-dependent J–V characteristics of ZnO/CdS/$CuGaSe_2$ single crystal solar cells. Sol. Energy Mater. Sol. C **77**, 415–422 (2003)
24. V.R. Reddy, S.K. Upadhyay, A. Gupta, A.M. Awasthi, S. Hussain, Enhanced dielectric and ferroelectric properties of $BaTiO_3$ ceramics prepared by microwave assisted radiant hybrid sintering. Ceram. Int. **40**, 8333–8339 (2014)
25. H.G. Cetinkaya, H. Tecimer, H. Uslu, S. Altindal, Photovoltaic characteristics of Au/PVA (Bi-doped)/n-Si Schottky barrier diodes (SBDs) at various temperatures. Curr. Appl. Phys. **13**, 1150 (2013)
26. A. Buyukbaş Uluşan, S. Altındal Yerişkin, A. Tataroğlu, M. Balbaşı, Y. Azizian Kalandaragh, Electrical and impedance properties of MPS structure based on (Cu_2O–CuO-PVA) interfacial layer. J. Mater. Sci. **29**, 8234–8243 (2018)
27. V.R. Reddy, Electrical properties of Au/polyvinylidene fluoride/n-InP Schottky diode with polymer interlayer. Thin Solid Films **556**, 300–306 (2014)
28. H. Tecimer, S.O. Tan, Ş. Altindal, Frequency-dependent admittance analysis of the MS structure with an interlayer of Zn-doped organic polymer nanocomposites. IEEE Trans. Electron Devices **65**, 231–236 (2018)
29. S.O. Tan, H. Tecimer, O. Cicek, Comparative investigation on the effects of organic and inorganic interlayers in Au/n-GaAs Schottky diodes. IEEE Trans. Electron Devices **64**, 984–990 (2017)
30. A.F. Özdemir, D.A. Aldemir, A. Kökce, S. Altindal, Electrical properties of Al/conducting polymer (P_2ClAn)/p-Si/Al contacts. Synth. Met. **159**, 427–1432 (2009)
31. A. Buyukbas-Ulusan, S. Altındal-Yerişkin, A. Tataroğlu, Forward and reverse bias current–voltage (I–V) characteristics in the metal–ferroelectric–semiconductor (Au/$SrTiO_3$/n-Si) structures at room temperature. J. Mater. Sci. **29**, 16740–16746 (2018)
32. S. Nezhadesm-Kohardafchahi, S. Farjami-Shayesteh, Y. Badali, Ş. Altındal, M.A. Jamshidi-Ghozlu, Y. Azizian-Kalandaragh, Formation of ZnO nanopowders by the simple ultrasound-assisted method: exploring the dielectric and electric properties of the Au/(ZnO-PVA)/n-Si Structure. Mater. Sci. Semicond. Process. **86**, 173–180 (2018)
33. E. Ahadi Akhlaghi, Y. Badali, S. Altindal, Y. Azizian-Kalandaragh, Preparation of mixed copper/PVA nanocomposites as an interface layer for fabrication of Al/Cu-PVA/p-Si Schottky structures. Phys. B **546**, 93–98 (2018)
34. U. Aydemir, İ. Taşçıoğlu, Ş. Altındal, İ. Uslu, A detailed comparative study on the main electrical parameters of Au/n-Si and Au/PVA: Zn/n-Si Schottky barrier diodes. Mater. Sci. Semicond. Process. **16**, 1865–1872 (2013)
35. A. Kaya, E. Marıl, Ş. Altındal, İ. Uslu, The comparative electrical characteristics of Au/n-Si (MS) diodes with and without a 2% graphene cobalt-doped $Ca_3Co_4Ga_{0\cdot001}O_x$ interfacial layer at room temperature. Microelectron. Eng. **149**, 166–171 (2016)
36. E. Arslan, S. Bütün, Y. Şafak, H. Uslu, İ. Taşçıoğlu, Ş. Altındal, E. Özbay, Electrical characterization of MS and MIS structures on AlGaN/AlN/GaN heterostructures. Microelectron. Reliab. **51**, 370–375 (2011)
37. V.R. Reddy, Electrical and interfacial properties of Au/n-InP Schottky contacts with nickel phthalocyanine (NiPc) interlayer. Indian J. Phys. **89**, 463–469 (2015)
38. B. Şahin, H. Çetin, E. Ayyildiz, The effect of series resistance on capacitance- voltage characteristics of Schottky barrier diodes. Solid State Commun. **135**, 490–495 (2005)
39. A. Kaya, S. Alialy, S. Demirezen, M. Balbaşı, S.A. Yerişkin, A. Aytimur, The investigation of dielectric properties and ac conductivity of Au/GO-doped PrBaCoO nanoceramic/n-Si capacitors using impedance spectroscopy method. Ceram. Int. **42**, 3322–3329 (2016)
40. İ. Taşçıoğlu, W.A. Farooq, R. Turan, Ş. Altındal, F. Yakuphanoğlu, Charge transport mechanisms and density of interface trapsin MnZnO/p-Si diodes. JALCOM **590**, 157–161 (2014)
41. M. Soylu, F. Yakuphanoğlu, Barrier height enhancement and temperature dependenceof the electrical characteristics of Al Schottky contacts on p-GaAs with organic rhodamine B interfacial layer. Superlattices Microstruct. **52**(3), 470–483 (2012)
42. S. Alptekin, Ş. Altındal, A comparative study on current/capacitance: voltage characteristics of Au/n-Si (MS) structures with and without PVP interlayer. J. Mater. Sci. **30**, 6491–6499 (2019)

Publisher's Note Springer Nature remains neutral with regard to jurisdictional claims in published maps and institutional affiliations.